processes

MDPI

Article

A Sustained-Release Material for Removing Aniline from Groundwater Based on Waste Foamed Polystyrene as the Encapsulating Matrix

Qizhi Zhu [1,†], Fanbin Meng [1,†], Yuning Yang [1], Bing Qin [1,*], Yushan Shi [2], Chuan Liang [1] and Feng Zhang [1]

[1] SINOPEC Research Institute of Petroleum Processing Co., Ltd., Beijing 100083, China; zhuqz627@163.com (Q.Z.); mengfanbin.ripp@sinopec.com (F.M.); yangyuning.ripp@sinopec.com (Y.Y.); liangchuan.ripp@sinopec.com (C.L.); zhangfeng.ripp@sinopec.com (F.Z.)
[2] School of Chemical Engineering and Technology, Dalian University of Technology, Dalian 116000, China; shiyushan@mail.dlut.edu.cn
* Correspondence: qinbing.ripp@sinopec.com
† These authors contributed equally to this work.

Abstract: In this study, a novel slow-release material using recycled waste foamed polystyrene (WFPS) as the carrier was developed for the degradation of aniline-contaminated groundwater. Sodium persulfate (SPS) and zero-valent iron (ZVI) were embedded in WFPS, enabling the controlled and sustained release of reactive species. Systematic investigations were conducted to optimize the material's composition and evaluate its performance under various conditions, including pH, initial aniline concentration, and the presence of common groundwater anions. The results revealed that the slow-release material effectively enhanced aniline degradation, achieving a maximum removal rate of 93.45% under flowing conditions. The degradation pathway was analyzed using GC-MS, identifying intermediates such as benzoquinone, hydroquinone, and dodecane, with eventual mineralization into CO_2 and H_2O. The material demonstrated robust performance, offering an efficient, cost-effective, and environmentally sustainable approach for in situ groundwater remediation.

Keywords: sustained-release material; aniline; groundwater; sodium persulfate

Academic Editor: Andrea Petrella

Received: 24 December 2024
Revised: 31 January 2025
Accepted: 5 February 2025
Published: 7 February 2025

Citation: Zhu, Q.; Meng, F.; Yang, Y.; Qin, B.; Shi, Y.; Liang, C.; Zhang, F. A Sustained-Release Material for Removing Aniline from Groundwater Based on Waste Foamed Polystyrene as the Encapsulating Matrix. *Processes* **2025**, *13*, 446. https://doi.org/10.3390/pr13020446

1. Introduction

Aniline is one of the most important amine compounds, widely used in the production of dyes, pharmaceuticals, and resins [1] and as a rubber vulcanization accelerator [2]. However, during industrial processes involving aniline, issues such as leakage, spills, and improper handling often occur, leading to significant groundwater contamination [3–5]. It is estimated that up to 30,000 tons of aniline are released into the environment each year as a result of illegal discharges of municipal and industrial wastewater and accidental spills [6]. As a priority organic pollutant, aniline is not only toxic to aquatic ecosystems but also poses serious health risks to humans, including methemoglobinemia and potential carcinogenic effects [7,8]. Typically, when people come into contact with low-concentration aniline wastewater (below 10 mg/L), aniline may cause mild irritant effects (hours to days), such as eye discomfort, skin redness, or itching. Long-term exposure at these levels (months to years) may lead to subtle neurological impairments, including headaches, dizziness, and memory loss. Between approximately 10 and 100 mg/L in water, aniline can cause more significant health issues. These include methemoglobinemia, where the blood's ability to carry oxygen is reduced, leading to symptoms of hypoxia [9]. These serious

health risks typically develop after exposure periods ranging from hours to days or weeks. When exposed to wastewater containing aniline concentrations exceeding 100 mg/L, it can result in severe acute toxicity. Symptoms may include respiratory distress, palpitations, chest pain, and potentially fatal outcomes. These extreme health risks can manifest within minutes to hours of exposure [10,11].

The Chinese Environmental Protection Ministry has imposed stringent regulations concerning aniline concentrations, specifically outlined in the "Discharge Standards of Water Pollutants for Dyeing and Finishing of Textile Industry" (GB 4287-2012) [12]. According to these standards, the textile industry is restricted to discharging aniline, either directly or indirectly, at a maximum concentration of 1 mg/L. Given its environmental persistence and hazardous nature, effective remediation of aniline-contaminated groundwater is a critical environmental challenge.

Advanced oxidation processes (AOPs), which generate highly reactive radicals for the degradation of organic pollutants, have become a widely studied and applied technology for groundwater remediation [13]. These processes are often combined with in situ methods such as permeable reactive barriers (PRBs) and injection wells to enhance their applicability in real-world scenarios [14,15]. Sodium persulfate (SPS) is one of the most commonly used oxidants in AOPs due to its ability to produce sulfate radicals ($\cdot SO_4^-$) with a high redox potential (2.5–3.1 V), which are effective in breaking down a wide range of recalcitrant organic pollutants [16].

Iron-based activation, particularly using zero-valent iron (ZVI), is a highly efficient and practical method to enhance SPS activity [17]. ZVI not only facilitates the generation of sulfate radicals under mild conditions but also provides sustained activation, ensuring a prolonged remediation effect [18]. This approach is cost-effective and environmentally friendly, making it suitable for large-scale applications.

Despite these advantages, the direct application of ZVI and SPS in groundwater systems can lead to the rapid consumption of reactive species, non-selective oxidation, and secondary contamination due to excessive chemical dosages [19–21]. Embedded slow-release materials offer a promising solution by encapsulating ZVI and SPS within a carrier matrix, thereby enabling controlled and prolonged release of reactive species in the targeted treatment zone [22–24]. This approach reduces the non-selective consumption of oxidants, minimizes secondary pollution, and enhances the overall efficiency and sustainability of the remediation process [25–27].

Polystyrene (PS), a widely used polymer derived from styrene monomers, has become one of the top five general-purpose synthetic resins globally, with an annual production exceeding 18 million tons [28–30]. The melting temperature of PS stands at 240 °C, with a water absorption rate ranging from 0.03 to 0.1. It demonstrates outstanding thermal stability and moisture resistance. Its widespread usage has led to the accumulation of waste foamed polystyrene (WFPS), which poses significant environmental challenges [31,32]. WFPS is non-biodegradable and, when incinerated, releases toxic substances such as styrene and benzene derivatives, contributing to air pollution and health hazards [33–35]. Conventional disposal methods, including landfilling and burning [36], are neither suitable nor sustainable for managing WFPS [37,38]. As a result, effective recycling and repurposing of WFPS have become a key focus for governments and researchers worldwide [39].

Polystyrene's excellent chemical stability, low reactivity with encapsulated agents, and swelling behavior in the presence of oils make it a highly suitable matrix for embedding reactive substances [40,41]. Moreover, leveraging recycled WFPS for creating slow-release materials not only aligns with the principles of sustainable development but also represents an innovative strategy to achieve "waste-to-resource" transformation.

In this study, we developed a novel slow-release material using recycled WFPS as the carrier. The WFPS was employed to encapsulate ZVI and SPS. This composite material enables the synergistic effects of ZVI and SPS to generate sulfate radicals in a controlled manner, targeting the degradation of aniline pollutants in groundwater. The degradation efficiency, activation mechanisms, and operational stability of the material under various conditions were systematically evaluated (Figure 1). This work aims to provide a sustainable, efficient, and cost-effective approach for the in situ remediation of aniline-contaminated groundwater, contributing to the advancement of green environmental technologies.

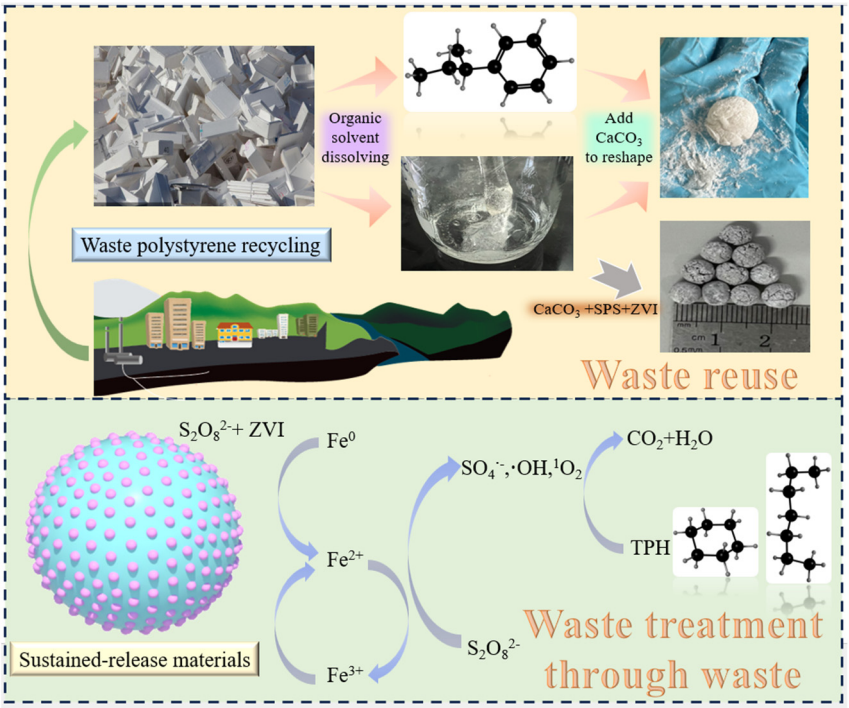

Figure 1. A diagram of the whole process and degradation mechanism in this experiment.

2. Materials and Methods

2.1. Materials

Waste foamed polystyrene (WFPS) was sourced from ordinary household waste. Ethyl acetate ($C_4H_8O_2$, ≥99.7%), dichloromethane (CH_2Cl_2, ≥99.7%), cyclohexane (C_6H_{12}, ≥99.7%), sodium chloride (NaCl, ≥99.7%), sodium bicarbonate ($NaHCO_3$, ≥99.7%), sodium carbonate (Na_2CO_3, ≥99.7%), sodium persulfate ($Na_2S_2O_8$, ≥99.7%), methanol (CH_3OH, ≥99.9%), potassium sulfate (K_2SO_4, ≥99.7%), and sodium hydroxide (NaOH, ≥96%) were procured from InnoChem Science & Technology Co., Ltd. (Beijing, China). Tetrachloroethylene (C_2Cl_4, ≥99.5%) was supplied by Aoran Fine Chemical Research Institute (Tianjin, China), while carbon tetrachloride (CCl_4, ≥99.7%), calcium carbonate ($CaCO_3$, 99.5%), and magnesium silicate adsorbent ($MgSiO_3$, ≥99.7%) were obtained from Aladdin Biochemical Technology Co., Ltd. (Shanghai, China). Anhydrous sodium sulfate (Na_2SO_4, ≥99.7%) was purchased from Macklin Biochemical Technology Co., Ltd. (Shanghai, China). Zero-valent iron (Fe^0, 99.9%) powder was supplied by Xindun Alloy Welding Material Spraying Co., Ltd. (Nangong, China). Sulfuric acid (H_2SO_4, ≥99.8%) was obtained from Xilong Scientific Co., Ltd. (Shantou, China). All reagents were used without further purification. Deionized water, deoxygenated prior to use, was utilized throughout the study.

Aniline (C_6H_7N, ≥99.7%), purchased from InnoChem Science & Technology Co., Ltd. (Beijing, China), was selected as the target contaminant for this research. Simulated pollu-

tant solutions with varying concentrations of aniline were prepared by dissolving predetermined amounts of aniline in deoxygenated water.

2.2. Preparation of Slow-Release Materials

The preparation of the slow-release materials involved the following steps. First, WFPS was pre-treated by crushing the recycled foam boards into small pieces, approximately 2 cm in length and width. These pieces were thoroughly cleaned with hot lye, rinsed, and dried. The cleaned WFPS fragments were then placed in a 2000 mL beaker for further processing.

Next, SPS, ZVI, calcium carbonate, and pre-treated WFPS were combined in specific proportions and mixed uniformly under well-ventilated conditions (Table 1). Then, 5 mL of organic solvent (take 4 g WFPS as an example) was gradually added to the mixture while continuously stirring until a fibrous consistency was achieved. The resultant mixture was passed through a tablet press to form cake-shaped structures, which were subsequently processed using a striping machine (LG-18, Baixin Pharmaceutical Machinery Co., Ltd., Ruian, China) to cut and roll the material into uniform strips.

Table 1. Nomenclature for (SPS+ZVI)/WFPS samples fabricated under various preparation conditions.

Sample No.	m (ZVI)	m (SPS)	m (Calcium Carbonate)	m (WFPS)	Organic Solvent	Nomenclature
1	0.8 g	4 g	12 g	4 g	Tetrachloroethylene	(SPS+ZVI)/WFPS-1
2	0.8 g	4 g	12 g	4 g	Ethyl acetate	(SPS+ZVI)/WFPS-2
3	0.8 g	4 g	12 g	4 g	Dichloromethane	(SPS+ZVI)/WFPS-3
4	0.8 g	4 g	12 g	4 g	Carbon tetrachloride	(SPS+ZVI)/WFPS-4

The strips were then placed horizontally in a tablet press and further shaped into spherical balls. Any balls with cracks or uneven shapes were discarded, and the remaining intact spheres were dried in a hot-air dryer at 60 °C for three hours (SHX2-150, Taiste Instrument Co., Ltd., Tianjin, China). The dried balls were then placed in a cool, dry area to air-dry naturally. The final product consisted of gray spheres with a diameter of 5–8 mm.

The prepared sample was designated as (SPS+ZVI)/WFPS. The preparation parameters and Nomenclature for the samples used in this study are summarized in Table 1.

2.3. Batch Experiments

Batch experiments were conducted to determine the optimal composition of the (SPS+ZVI)/WFPS material and to evaluate the influence of external factors on its pollutant degradation performance. A 500 mL solution of aniline (100 mg/L), prepared using ultrapure water, was placed in a conical flask and maintained at room temperature. A 5 g sample of the prepared embedding material was added to the solution for a static reaction, and aliquots were collected at predetermined intervals based on the experimental design.

The experiments investigated the effects of various factors on the degradation efficiency of aniline, including different organic solvents, the initial concentration of aniline, the presence of common anions in groundwater, and variations in pH. These parameters were systematically varied to assess their impact on the degradation kinetics and to identify the optimal operating conditions.

2.4. Column Experiment

Column experiments were conducted to investigate the degradation performance of the (SPS+ZVI)/WFPS-2 material on aniline under flowing conditions. A plexiglass column (300 mm in height and 30 mm in internal diameter) was used as the experimental apparatus. To ensure uniform water distribution and simulate a one-dimensional dynamic

groundwater environment, quartz sand with a particle size of 1–2 mm was packed into the column.

The slow-release material was placed at the center of the column, surrounded by glass beads. A benzene-contaminated water sample with an initial aniline concentration of 25 mg/L was prepared, and the system was operated with an upward water flow at a hydraulic flow rate of 1.0 mL/min. The total dosage of the slow-release material was 100 g. The experiment was conducted for 7 days, with samples collected and analyzed at predetermined intervals to monitor the degradation of aniline.

2.5. Analyze Methods

The degradation rate of aniline was analyzed using high-performance liquid chromatography (HPLC, LC-20AT, Shimadzu, Kyoto, Japan). Test conditions were C 18 (150 mm × 4.6 mm, 5 μm), a column temperature of 30 °C, a mobile phase of 40% methanol and 60% ultrapure water solution, a flow rate of 1.0 mL/min, a sample volume of 10 μL, and a measurement wavelength λ = 280 nm.

The degradation products were identified using gas chromatography–mass spectrometry (GC-MS, 7890A GC-5975C MS, Agilent Technologies, Santa Clara, CA, USA). Chromatography was performed on an HP-5MS column (30.0 mm × 250 μm, 0.25 μm). The initial temperature was maintained at 40 °C for 2 min, increased to 250 °C for 3 min at 8 °C/min, and increased to 300 °C for 5 min at 15 °C/min. Gasification chamber temperature 250 °C; transmission line temperature 300 °C; carrier gas He; carrier gas flow rate 1.0 mL/min; no diversion.

Mass spectrum conditions: EI source; electron energy 70 eV; ion source temperature 230 °C; quadrupole 150 °C; scan mode SCAN. The scanning quality ranges from 20 to 500 u.

2.6. Characterizations

The morphological changes in the (SPS+ZVI)/WFPS-2 material before and after the reaction were observed using scanning electron microscopy (SEM, SU8010, Hitachi Limited, Tokyo, Japan).

X-ray diffraction (XRD, K-Alpha, Thermo Fisher Scientific, Waltham, MA, USA) with a copper (Cu) target was used to analyze the composition of the (SPS+ZVI)/WFPS-2 material before and after the reaction. The scanning range was 10–80°, with a scanning speed of 2°/min.

The elemental composition and valence states of the material's surface before and after the reaction were investigated using X-ray photoelectron spectroscopy (XPS, D8 Advance, Bruker, Karlsruhe, Germany).

The specific surface area, total pore volume, and porosity of the (SPS+ZVI)/WFPS-2 material before and after the reaction were measured using a BET surface area analyzer (ASAP 2460, Micromeritics, Norcross, GA, USA).

3. Results and Discussion

3.1. Selection of Organic Solvent for Material Preparation

Although waste foamed polystyrene (WFPS) is soluble in various organic solvents, selecting the most suitable solvent for reprocessing into slow-release materials is critical for optimizing cost, extending the reaction cycle, and minimizing potential secondary pollution caused by the solvents. Based on a literature review, four commonly used organic solvents capable of dissolving WFPS were selected for material preparation, and their performance was evaluated through static batch experiments.

The experimental results are shown in Figure 2. During a 7-day (168 h) static reaction, the materials prepared with ethyl acetate and tetrachloroethylene demonstrated superior aniline removal efficiencies. The degradation rate of aniline by the material prepared with ethyl acetate reached 60.94%, while the material prepared with tetrachloroethylene achieved a comparable degradation rate of 61.86%.

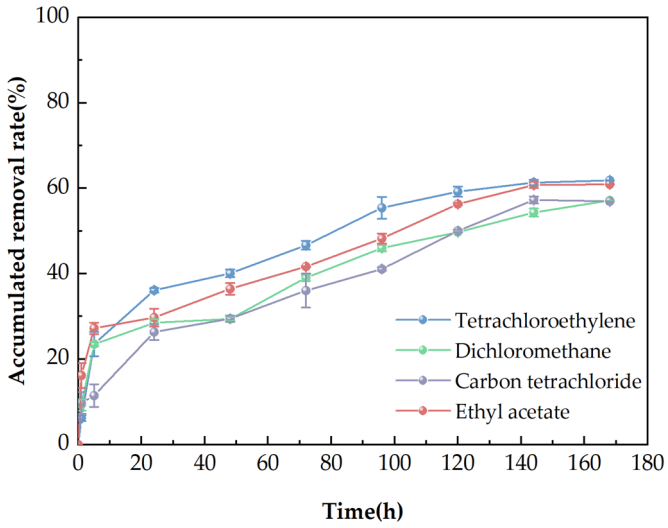

Figure 2. The influence of (SPS+ZVI)/WFPS prepared with different organic solvents on the degradation of aniline.

Considering the relatively low toxicity of ethyl acetate and the potential risks of environmental contamination from chlorinated hydrocarbons such as tetrachloroethylene [42], ethyl acetate was chosen as the solvent for subsequent material preparation. This choice balances environmental sustainability and material performance, aligning with the goal of developing green and efficient remediation technologies.

3.2. Morphological Changes Before and After Reaction

The SEM images reveal that the (SPS+ZVI)/WFPS-2 surface before the reaction is rough and dense, with a few micropores and visible particles adhering to the surface (Figure 3a,b). The cross-sectional images (Figure 3c,d) show the presence of cracks and distinct pore-like structures within the material, which facilitate water penetration. The embedded particles are well dispersed throughout the interior of the material, with no significant agglomeration observed. These structural characteristics are beneficial for the controlled release of active agents and the ingress of water into the material, ensuring efficient interaction between the oxidants and pollutants.

In contrast, the SEM images after the reaction (Figure 3e–h) exhibit significant morphological changes. The surface of the material displays markedly larger pores compared to the pre-reaction state. This change is attributed to the dissolution of surface oxidants upon contact with water, which creates pathways for water to penetrate the material's interior. As the reaction progresses, further dissolution of internal oxidants leads to the continuous formation of new pores, resulting in a highly porous structure after leaching.

The cross-sectional images (Figure 3g,h) further corroborate this observation, showing clear evidence of oxidant dissolution within the material upon exposure to water. The increased porosity and structural changes enhance the material's capacity for sustained pollutant degradation by facilitating water flow and ensuring prolonged contact with active agents. These results highlight the material's suitability for applications requiring long-term controlled release and efficient pollutant removal.

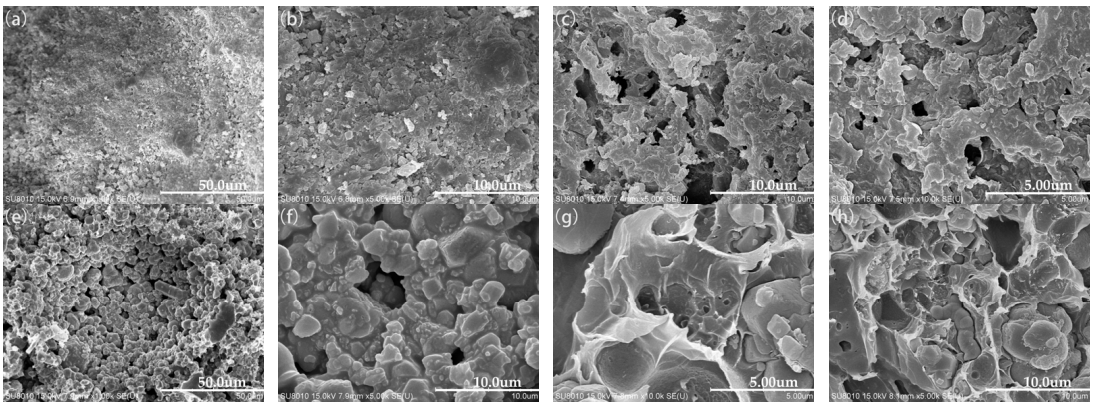

Figure 3. SEM images of the surface of (SPS+ZVI)/WFPS-2 before the reaction (**a**,**b**), the cross-section of (SPS+ZVI)/WFPS-2 before the reaction (**c**,**d**), the surface of (SPS+ZVI)/WFPS-2 after the reaction (**e**,**f**), and the cross-section of (SPS+ZVI)/WFPS-2 after the reaction (**g**,**h**).

3.3. Compositional Changes Before and After Reaction

The XRD patterns of the (SPS+ZVI)/WFPS-2 material before and after the reaction are shown in Figure 4. The primary crystalline phase identified in both the pre- and post-reaction samples was $CaCO_3$, with strong diffraction peaks observed at 2θ = 29.4°, 39.41°, and 48.51°, corresponding to the (104), (113), and (116) planes of hexagonal $CaCO_3$ (PDF 99-0022).

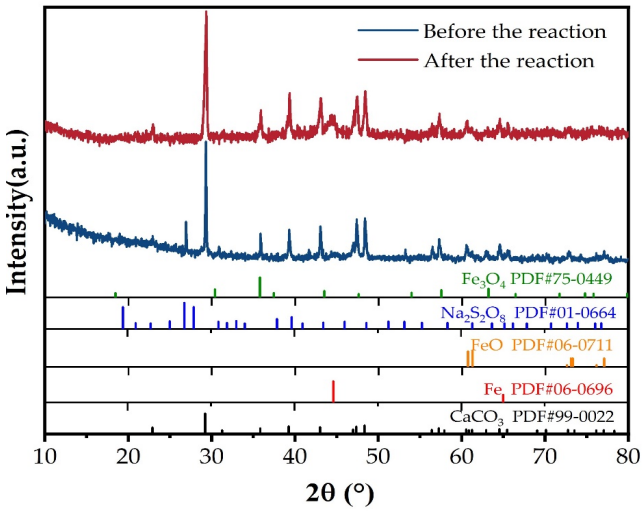

Figure 4. XRD results for (SPS+ZVI)/WFPS-2 before and after the reaction.

It is worth noting that the peak strength of $CaCO_3$ in the sample after the reaction has no significant change from that before the reaction. This may be due to the high amount of $CaCO_3$ used in the preparation process. After the reaction, the surfaces of the materials have mostly released their SPS and ZVI contents, at which point the relative content of $CaCO_3$ significantly increases, potentially leading to an elevated diffraction peak intensity of $CaCO_3$ in the post-reaction analysis. In addition to the $CaCO_3$ peaks, a noticeable increase in the intensity of the diffraction peak at 2θ = 44.67° was observed in the post-reaction sample. This peak corresponds to the (110) plane of cubic-phase iron (Fe), indicating an increased presence of iron on the material's surface after the reaction. This observation suggests that zero-valent iron (ZVI), initially embedded within the material, gradually migrated to the surface during the reaction process. The continuous release of ZVI is beneficial for sustained pollutant degradation, as it serves as an activator of sodium

persulfate, generating reactive radicals for effective pollutant breakdown. This also led to a significant change in the SPS peaks in the samples after the reaction.

Notably, no reflection of polystyrene was detected. This is because polystyrene makes up only 19.23% of the overall composition. This relatively low concentration may render the amorphous halo in the XRD pattern insufficiently prominent, making it difficult to observe directly. In addition, this may also be due to the fact that polystyrene may exist in the form of amorphous or low crystallinity, which makes it difficult to observe significant diffraction peaks in the XRD pattern. Amorphous materials do not have long-range ordered structures, so they do not produce strong diffraction effects [43].

These XRD results confirm the structural and compositional changes in the (SPS+ZVI)/WFPS-2 material during the reaction. The observed reduction in $CaCO_3$ content and the increased surface availability of Fe highlight the material's dynamic release characteristics, which are crucial for maintaining its reactivity and efficacy in pollutant degradation over time.

3.4. X-Ray Photoelectron Spectroscopy (XPS) Analysis

The surface elemental composition of the (SPS+ZVI)/WFPS-2 material before and after the reaction was analyzed using XPS, and the results are shown in Figure 5. Before the reaction (Figure 5a), the dominant surface element was calcium. After the reaction (Figure 5b), the sodium and sulfur contents increased. This is likely due to the gradual leaching of sodium persulfate (SPS) as it dissolves in water, with unreacted SPS accumulating on the surface of the material particles. Additionally, nitrogen was detected on the post-reaction material surface, attributed to nitrogen-containing compounds formed as residual byproducts of aniline degradation.

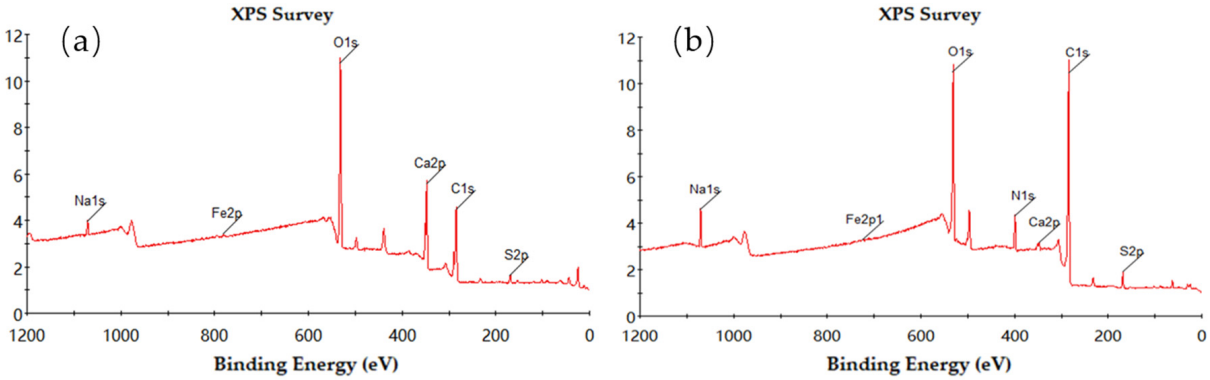

Figure 5. XPS results for the (SPS+ZVI)/WFPS-2 before (**a**) and after (**b**) the reaction.

The carbon content on the surface also increased significantly after the reaction. This increase can be explained by the detachment of surface particles, such as calcium carbonate, during the reaction process, leaving the polystyrene shell material exposed. This surface exposure resulted in a pronounced increase in carbon content detected in the XPS analysis.

Further analysis of the iron species (Figure 6) revealed notable changes in the chemical state of iron before and after the reaction. Prior to the reaction, the main iron species on the surface included Fe^{2+} and Fe^{3+}, with binding energies of 710.03 eV and 712.4 eV, respectively, and relative proportions of 53% and 47% (Table 2). This composition likely reflects the partial oxidation of zero-valent iron (ZVI) due to prolonged exposure to air during material preparation.

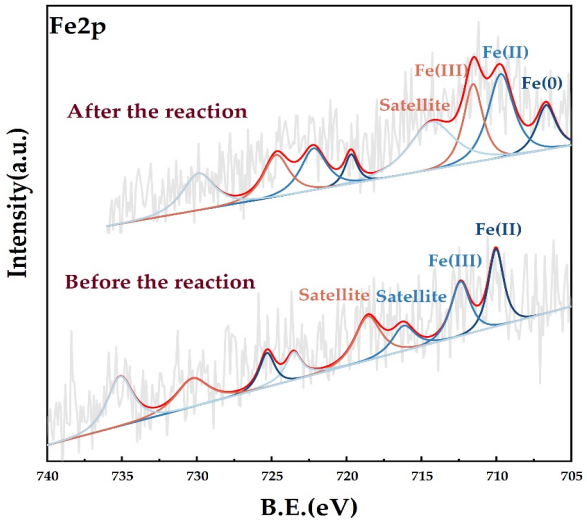

Figure 6. Morphology of iron element before and after reaction of (SPS+ZVI)/WFPS-2.

Table 2. Chemical state and peak parameters of iron.

Sample Name	Chemical State of Iron	Peak Area	Peak Area Proportion	Peak Position (eV)
Before the reaction	Fe^0	0	0	— —
	Fe^{2+}	787.3865	53%	710.03
	Fe^{3+}	688.9631	47%	712.4
After the reaction	Fe^0	582.1092	19%	706.67
	Fe^{2+}	1455.273	48%	709.7
	Fe^{3+}	1024.512	33%	711.55

After the reaction, the relative amount of Fe^{3+} increased significantly, with its peak area reaching 1.5 times that of the pre-reaction state. This increase is attributed to the rapid oxidation of ZVI to Fe^{3+} during the activation process of SPS, as described by reaction Equations (1)–(4). Additionally, a peak corresponding to Fe^0 was observed at a binding energy of 706.67 eV. The presence of Fe^0 is likely due to the effective encapsulation of ZVI within the material, preventing its oxidation until it was released to the surface during the reaction. The proportion of Fe^{2+} remained relatively stable at 48% post-reaction, as Fe^{2+} plays a critical role in activating SPS to generate reactive radicals for pollutant degradation [44].

These XPS results confirm the dynamic changes in surface composition during the reaction process. The observed trends in calcium, sulfur, sodium, and iron content further highlight the gradual release and activation mechanisms of the material, ensuring sustained reactivity and efficient aniline degradation.

$$Fe^{2+} + S_2O_8{}^{2-} \rightarrow Fe^{3+} + SO_4{}^{2-} + SO_4{}^{\cdot -} \quad (1)$$

$$Fe^{3+} + S_2O_8{}^{2-} \rightarrow Fe^{2+} + S_2O_8{}^{\cdot -} \quad (2)$$

$$Fe^{3+} + S_2O_8{}^{2-} + 2H_2O \rightarrow Fe^{2+} + HSO_5{}^{-} + 2H^{+} \quad (3)$$

$$Fe^{2+} - e^{-} \rightarrow Fe^{3+} \quad (4)$$

3.5. BET Pore Size Distribution Analysis

The BET pore size distribution results of the (SPS+ZVI)/WFPS-2 material before and after the reaction are shown in Figure 7. The specific surface areas before and after the reaction were 1.847 m^2/g and 2.594 m^2/g, respectively. Before the reaction, the material exhibited a relatively low pore volume, primarily due to the embedding of a significant number of particles on the material surface, which limited pore formation.

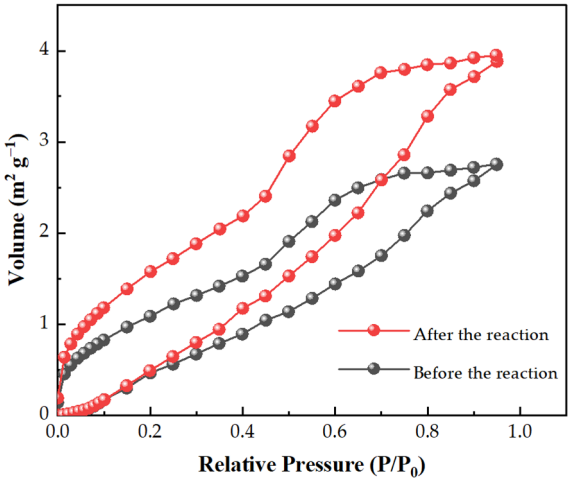

Figure 7. BET results for (SPS+ZVI)/WFPS-2 before and after the reaction.

After the material was immersed in water, the sodium persulfate particles embedded in the surface layer gradually dissolved, creating additional pores and increasing the pore volume. This enhanced porosity facilitated the gradual diffusion of the pollutant solution into the interior of the material spheres. The increased accessibility allowed sustained interactions between the pollutants and the reactive agents embedded within the material, ensuring continuous degradation reactions.

These findings highlight the dynamic structural evolution of the slow-release material during the reaction process. The increase in pore volume and connectivity enhances the material's efficiency by promoting the deeper penetration of pollutants and the prolonged activation of the embedded reactive agents, making it highly suitable for in situ remediation applications.

3.6. Effect of Initial Aniline Concentration on Degradation Performance

The degradation performance of the slow-release material at different initial aniline concentrations was investigated in a 7-day static batch experiment, and the results are presented in Figure 8. The degradation rate varied with the initial aniline concentration: for a 15 mg/L aniline solution, the degradation rate was 81.76%; for 25 mg/L, 85.29%; for 50 mg/L, 86.71%; and for 75 mg/L, 89.05%. At an initial concentration of 100 mg/L, the degradation rate was comparable to that of the 75 mg/L solution.

The results indicate that the degradation efficiency was lower for low-concentration aniline solutions compared to high-concentration solutions. This phenomenon may be attributed to the slower reaction kinetics in low-concentration systems, where the availability of reactive radicals is relatively excessive compared to the pollutant concentration, leading to less efficient utilization of the oxidants. In practical applications for groundwater remediation, this trend is consistent with the challenge of effectively degrading low-concentration organic pollutants [45].

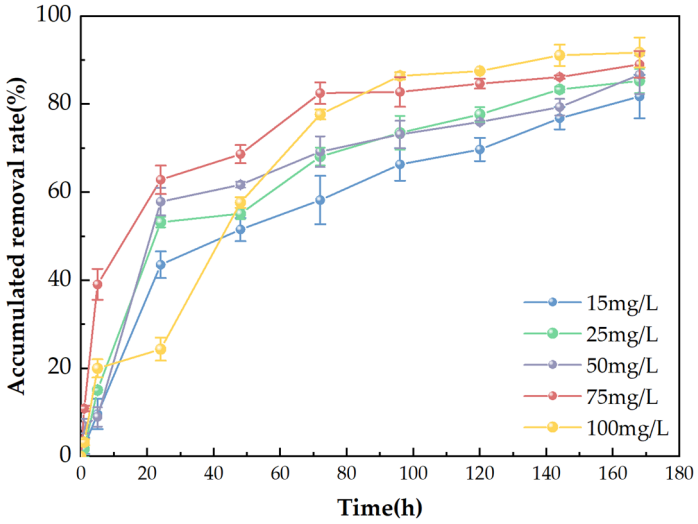

Figure 8. The effect of the initial aniline concentration on the degradation performance of (SPS+ZVI)/WFPS-2.

To achieve higher aniline removal rates and optimize the utilization of the reactive system, an initial aniline concentration of 100 mg/L was selected for subsequent experiments. This concentration ensures the efficient use of the oxidants while simulating the extremely high pollutant load conditions commonly encountered in contaminated groundwater.

3.7. Effect of Common Groundwater Anions on Aniline Degradation by Slow-Release Materials

The presence of common groundwater anions was found to have varying effects on the degradation of aniline by the slow-release material. As shown in Figure 9a,b, SO_4^{2-} and CO_3^{2-} had minimal impact on aniline removal, with degradation rates remaining above 89%. This stability suggests that these anions do not significantly interfere with the active radicals generated by the material. However, the addition of Cl^- led to a slight decrease in removal efficiency, with the degradation rate dropping to 80.51% at higher Cl^- concentrations (Figure 9c). As described by reaction Equations (5) and (6), this inhibition is likely due to the consumption of high-reactivity radicals ($\cdot SO_4^-$ and OH) by Cl, forming less reactive species such as ·Cl and $\cdot Cl_2^-$, which lower the overall oxidative capacity of the system.

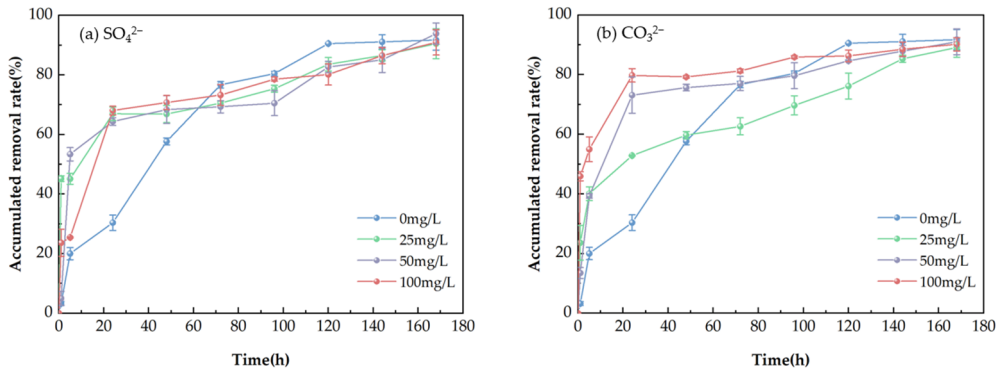

Figure 9. *Cont.*

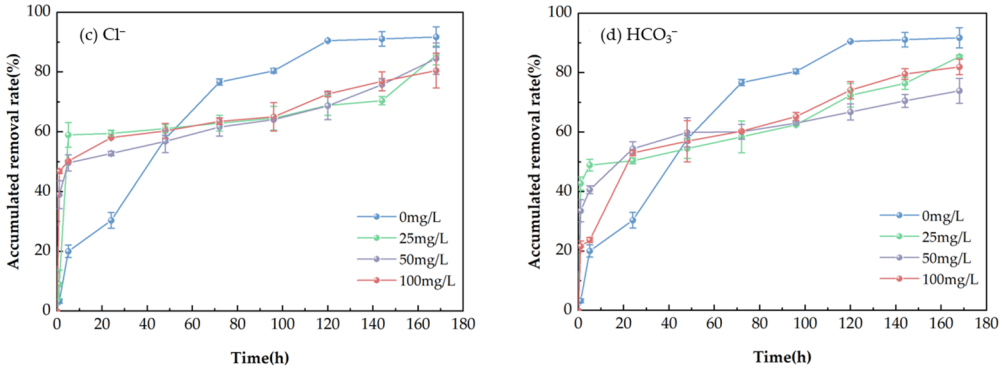

Figure 9. The influence of common groundwater anions on the aniline degradation concentration of (SPS+ZVI)/WFPS-2.

In contrast, HCO_3^- exhibited a more pronounced impact, reducing the degradation rate to 73.93% at 50 mg/L (Figure 9d). This effect is attributed to the formation of carbonate radicals, HCO_3^-, with lower reactivity, which slows the overall reaction kinetics. Interestingly, at 100 mg/L, the degradation rate rebounded slightly to 81.95%, likely due to the ability of $\cdot HCO_3^-$ to react with electron-rich compounds and its potential to catalyze SPS decomposition, generating additional $\cdot SO_4^-$. As described by reaction Equations (7) and (8), these results indicate that while certain anions can inhibit aniline degradation, the slow-release material remains effective under various groundwater conditions, showcasing its robustness for in situ remediation applications.

$$SO_4^- + Cl^- \rightarrow SO_4^{2-} + \cdot Cl \quad (5)$$

$$OH + \cdot Cl \rightarrow \cdot ClOH^- \quad (6)$$

$$OH + HCO_3^- \rightarrow \cdot CO_3^- + H_2O \quad (7)$$

$$SO_4^- + HCO_3^- \rightarrow \cdot HCO_3 + SO_4^{2-} \quad (8)$$

The pH of the solution plays a crucial role in the activation of persulfate and the subsequent oxidation of organic pollutants, as it affects both the distribution of reactive radicals and the speciation of target pollutants. To minimize interference from additional ions introduced by buffering agents, the solution pH was adjusted using NaOH and H_2SO_4. The effect of pH on aniline degradation is shown in Figure 10.

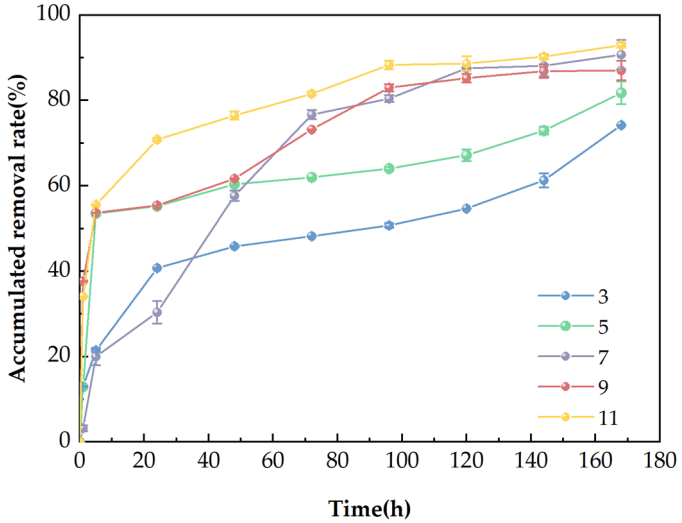

Figure 10. The influence of pH on the aniline degradation concentration of (SPS+ZVI)/WFPS-2.

As pH increased, the degradation efficiency of aniline improved. At pH values of 3, 5, 7, 9, and 11, the degradation rates were 74.22%, 81.78%, 90.75%, 87.03%, and 92.95%, respectively. The system showed lower degradation efficiency in strongly acidic conditions (pH = 3), while the highest efficiency was observed under strongly alkaline conditions (pH = 11). Among weakly acidic and weakly alkaline conditions (pH = 5, 7, and 9), the optimal degradation occurred at pH = 7, where the removal rate reached 90.75%.

This behavior can be attributed to the dominant radicals present under different pH conditions. In acidic environments (pH < 7), sulfate radicals ($\cdot SO_4^-$) are predominant, whereas hydroxyl radicals (·OH) dominate at higher pH values. Since OH has a higher redox potential compared to $\cdot SO_4^-$ [46], its presence at elevated pH levels enhances the oxidative capacity of the system. However, under neutral conditions (pH = 7), a balance between $\cdot SO_4^-$ and ·OH likely contributes to the efficient and sustained degradation of aniline, making it the optimal pH for pollutant removal in this study.

3.8. Aniline Degradation Performance of Slow-Release Materials in Flowing Conditions

The degradation performance of the slow-release material remained consistently high over the 7-day experiment (Figure 11). Initially, the aniline removal rate was relatively low, at only 34.49%. This lower initial efficiency can be attributed to the dissolution of surface-bound materials upon first contact with water. As indicated by the characterization results, the surface predominantly consisted of calcium carbonate, with limited amounts of SPS and ZVI. Consequently, the aniline concentration in the effluent was higher at the start of the reaction.

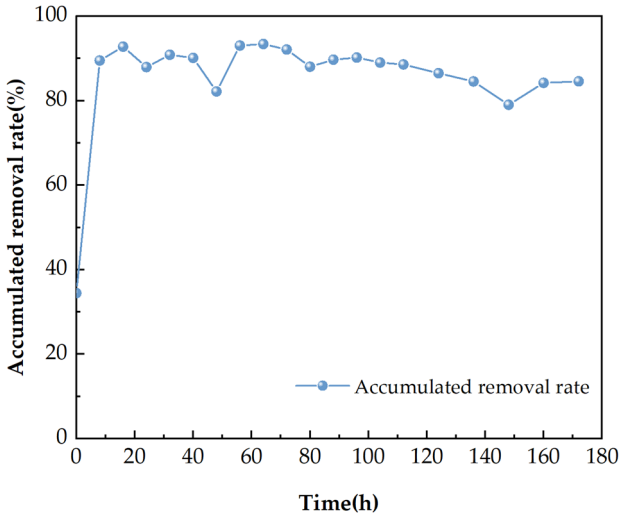

Figure 11. The aniline degradation performance of (SPS+ZVI)/WFPS-2 in flowing conditions.

The removal rate peaked at 93.45% after 64 h, as the flowing water facilitated penetration into the interior of the slow-release particles. This enhanced water access promoted the release of embedded reactive agents, such as SPS and ZVI, resulting in a more efficient degradation process. Notably, the flowing conditions provided better mixing and transport compared to static batch experiments, leading to higher overall removal rates.

By the end of the 7-day experiment, the aniline removal rate stabilized at 84.6%, with an average removal rate of 85.69% throughout the testing period. The steady performance and high removal efficiency demonstrate the material's suitability for degrading aniline pollutants in real-world groundwater environments under dynamic flow conditions.

3.9. Degradation Products and Pathways of Aniline

The degradation products of aniline were analyzed using GC-MS at 0 h, 48 h, and 168 h of the reaction, as shown in Figure 12. Aniline exhibited a distinct peak at 10.42 min. The primary intermediate products identified during the reaction were benzoquinone (21.76%), dodecane (6.57%), and hydroquinone (1.18%).

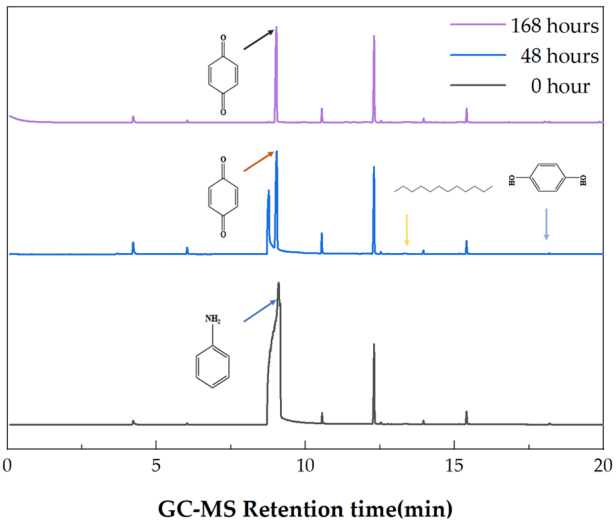

Figure 12. GC-MS results before and after the reaction.

The rapid decrease in aniline concentration over time and the formation of alkanes suggest that some intermediates underwent mineralization, leading to ring-opening reactions and the formation of linear carbon chains. As the alkyl carbon chains lengthened, their retention times in GC-MS analysis increased correspondingly. This indicates that the degradation process not only reduces aniline but also generates intermediates that are further oxidized into simpler and less toxic compounds.

Based on the intermediates detected, Figure 13 illustrates a plausible degradation pathway for aniline. The process initiates with radicals formed in the reaction system attacking the benzene ring of aniline, resulting in hydroxylation and the subsequent formation of aminophenol. This is followed by a substitution reaction involving the amino group, yielding phenol, which can then be further oxidized to hydroquinone. Subsequently, hydroquinone undergoes dehydrogenation to form benzoquinone. Benzoquinone ultimately undergoes mineralization, resulting in the ring-opening formation of straight-chain alkanes or conversion into CO_2 and H_2O. However, it is noteworthy that the formation of linear alkanes as mineralization byproducts is not as evident as observed after 168 h of GC-MS analysis. This may indicate that the generated benzoquinone has not been completely decomposed yet. Nevertheless, due to its poor stability, benzoquinone will eventually be decomposed into CO_2 and H_2O during the long-term process of complete mineralization [47].

This degradation pathway highlights the material's effectiveness in breaking down complex organic pollutants like aniline into simpler and less harmful products, demonstrating its potential for practical applications in groundwater remediation.

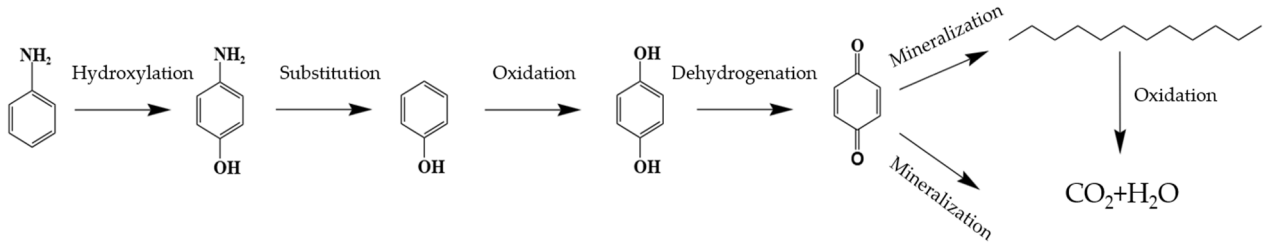

Figure 13. Potential degradation pathways of aniline.

4. Conclusions

This study successfully developed a slow-release material using recycled WFPS for the remediation of aniline-contaminated groundwater. The material, optimized with ethyl acetate as the solvent, demonstrated consistent and high degradation efficiency in both static and flowing conditions. The gradual release of embedded reactive agents allowed the efficient activation of sodium persulfate, sustaining pollutant degradation over extended periods. Experimental results highlighted the material's adaptability to varying groundwater conditions, including changes in pH, anion composition, and pollutant concentration.

When the initial concentration of aniline was 100 mg/L, the degradation rate reached 91.75% after 168 h. In the experiment, SO_4^{2-} and CO_3^{2-} had no obvious inhibitory effects on the removal of aniline, while Cl^- and HCO_3^- reduced the removal rate. It was found that alkaline conditions were more conducive to the degradation of pollutants. By adjusting the pH value to the alkaline range, the degradation efficiency of AN could be significantly improved. Over the 7-day flow experiment, the aniline removal rate started at 34.49% but peaked at 93.45%. By the end of the 7-day experiment, the aniline removal rate stabilized at 84.6%, with an average removal rate of 85.69% throughout the testing period. The consistently high degradation performance demonstrates the material's suitability for aniline pollutant removal in groundwater under dynamic flow conditions.

The degradation pathway of aniline was elucidated, showing progressive transformation into intermediates such as benzoquinone and hydroquinone, followed by mineralization into CO_2 and H_2O. These findings underscore the material's potential for practical applications in groundwater remediation, combining high efficacy with environmental sustainability.

In future work, we will thoroughly investigate enhancement strategies for material recyclability. This will encompass the development of novel composite material components that are readily separable, the optimization of processing techniques to minimize the environmental footprint of composite waste, and the exploration of reuse pathways for composite waste materials, thereby enhancing the practicality of the material, enabling it to better tackle broader environmental pollution issues.

Author Contributions: Conceptualization, Q.Z.; methodology, Y.S.; formal analysis, Q.Z.; investigation, Y.Y.; writing original draft, Q.Z.; writing review and editing, F.M.; supervision, B.Q.; software, C.L.; project administration, F.M.; funding acquisition, F.M.; visualization, F.Z. All authors have read and agreed to the published version of the manuscript.

Funding: This research was funded by the National Natural Science Foundation of China (grant number 42207083) and the Project of SINOPEC (No. 324099).

Data Availability Statement: Data are contained within the article.

Conflicts of Interest: Authors Qizhi Zhu, Fanbin Meng, Yuning Yang, Bing Qin, Chuan Liang and Feng Zhang were employed by SINOPEC Research Institute of Petroleum Processing Co., Ltd. The remaining authors declare that the research was conducted in the absence of any commercial or financial relationships that could be construed as a potential conflict of interest.

References

1. Jiang, Y.; Li, X.; Qin, Z.; Ji, H. Preparation of ni/bentonite catalyst and its applications in the catalytic hydrogenation of nitrobenzene to aniline. *Chin. J. Chem. Eng.* **2016**, *24*, 1195–1200. [CrossRef]
2. Zhu, J.; Yao, J.; Cao, Y.; Pang, W.; Knudsen, T.; Liu, J. Degradation of aniline via microbial treated post Fe(II) or Co(II)/PMS advanced oxidation processes. *Sep. Purif. Technol.* **2025**, *359*, 130809. [CrossRef]
3. Dong, H.; Liu, H.; Yang, X.; Gong, H.; Zhang, H.; Wang, R.; Yan, L.; Mai, W. The effect of initial conditions with aerobic biological treatment on aniline dyeing wastewater. *Processes* **2021**, *9*, 1329. [CrossRef]
4. Cao, W.; Wen, Z.; Li, S.; Ren, Y.; Nan, T.; Li, X. Remediation of aniline-contaminated aquifer by combining in-well rhizobium borbori and circulated groundwater electrolysis. *J. Hazard. Mater.* **2024**, *465*, 133046. [CrossRef] [PubMed]
5. Mustapha, N.A.; Liu, H.; Ibrahim, A.O.; Huang, Y.; Liu, S. Degradation of aniline in groundwater by persulfate with natural subsurface sediment as the activator. *Chem. Eng. J.* **2020**, *417*, 128078. [CrossRef]
6. Sheng, J.; Xu, J.; Qin, B.; Jiang, H. Three-dimensional flower-like magnetic CoFe-LDHs/$CoFe_2O_4$ composites activating peroxymonosulfate for high efficient degradation of aniline. *J. Environ. Manag.* **2022**, *310*, 114693. [CrossRef] [PubMed]
7. Gao, R.; Zhu, J.; Xi, B.; Wang, Y.; Bai, S.; Wang, Y. Effect of pumping-induced soil settlement on the migration and transformation of aniline. *Chemosphere* **2024**, *352*, 141361. [CrossRef] [PubMed]
8. Mohammed, M.; Mekala, L.P.; Chintalapati, S.; Chintalapati, V.R. New insights into aniline toxicity: Aniline exposure triggers envelope stress and extracellular polymeric substance formation in Rubrivivax benzoatilyticus JA2. *J. Hazard. Mater.* **2020**, *385*, 121571. [CrossRef]
9. Makhdoumi, P.; Hossini, H.; Ashraf, M.; Limoee, M. Molecular Mechanism of Aniline Induced Spleen Toxicity and Neuron Toxicity in Experimental Rat Exposure: A Review. *Curr. Neuropharmacol.* **2019**, *17*, 201–213. [CrossRef] [PubMed]
10. Feng, Y.; Chen, L.; Zhang, T.; Wu, Y.; Song, L.; Wang, Y. Research progress on health effects of aniline. *Chin. J. Prev. Med.* **2020**, *54*, 213–218. [CrossRef]
11. Soni, B.; Sherertz, E. Contact dermatitis in the textile industry: A review of 72 patients. *Am. J. Clin. Dermatol.* **1996**, *7*, 226–230. [CrossRef]
12. Liu, Y.; Zhang, H.; Sun, J.; Liu, J.; Xue, S.; Zhang, J.; Zhang, A.; Ognier, S.; Cavadias, S.; Li, P. Degradation of aniline in aqueous solution using non-thermal plasma generated in microbubbles. *Chem. Eng. J.* **2018**, *345*, 679–687. [CrossRef]
13. Zhou, Y.; Xiang, Y.; He, Y.; Yang, Y.; Zhang, J.; Luo, L.; Peng, H.; Dai, C.; Zhu, F.; Tang, L. Applications and factors influencing of the persulfate-based advanced oxidation processes for the remediation of groundwater and soil contaminated with organic compounds. *J. Hazard. Mater.* **2018**, *359*, 396–407. [CrossRef] [PubMed]
14. Sakr, M.; El Agamawi, H.; Klammler, H.; Mohamed, M.M. A review on the use of permeable reactive barriers as an effective technique for groundwater remediation. *Groundw. Sustain. Dev.* **2023**, *21*, 100914. [CrossRef]
15. Dai, C.; Zhang, J.; Zou, J.; Hu, J.; Gao, T.; Li, Z.; Liang, Y.; Zhou, L. Activated carbon/persulfate-driven in-situ remediation of naphthalene-polluted groundwater: Insights into active sites, passivation-activation mechanisms and practical applications. *J. Environ. Chem. Eng.* **2024**, *12*, 113126. [CrossRef]
16. Singh, R.; Chakma, S.; Birke, V. Performance of field-scale permeable reactive barriers: An overview on potentials and possible implications for in-situ groundwater remediation applications. *Sci. Total. Environ.* **2023**, *858*, 158838. [CrossRef]
17. Wu, Q.; Sun, Y.; Luo, Z.; Li, X.; Wen, Y.; Shi, Y.; Wu, X.; Huang, X.; Zhu, Y.; Huang, C. Application and development of zero-valent iron (ZVI)-based materials for environmental remediation: A scientometric and visualization analysis. *Environ. Res.* **2024**, *241*, 117659. [CrossRef] [PubMed]
18. Zeng, X.; Wang, L.; Zhang, Y.; Zhou, S.; Yu, Z.; Liu, X.; Chen, C. Enhanced removal of organic pollutants by ball-milled FeS/ZVI activated persulfate process: Characterization, performance, and mechanisms. *Surf. Interfaces* **2022**, *29*, 101697. [CrossRef]
19. Faisal, A.A.H.; Sulaymon, A.H.; Khaliefa, Q.M. A review of permeable reactive barrier as passive sustainable technology for groundwater remediation. *Int. J. Environ. Sci. Technol.* **2018**, *15*, 1123–1138. [CrossRef]
20. Wei, K.; Ma, J.; Xi, B.; Yu, M.; Cui, J.; Chen, B.; Li, Y.; Gu, Q.; He, X. Recent progress on in-situ chemical oxidation for the remediation of petroleum contaminated soil and groundwater. *J. Hazard. Mater.* **2022**, *432*, 128738. [CrossRef]
21. Zhao, B.; Sun, Z.; Liu, Y. An overview of in-situ remediation for nitrate in groundwater. *Sci. Total. Environ.* **2022**, *804*, 149981. [CrossRef] [PubMed]
22. Sheng, L.; Zhang, H.; Ding, M. Preparation of core-shell composite materials capable of slowly releasing phosphate and their remediation performance of uranium-contaminated groundwater. *Chemosphere* **2023**, *344*, 140160. [CrossRef] [PubMed]
23. Yoo-iam, M.; Satapanajaru, T.; Chokejaroenrat, C.; Sakulthaew, C.; Comfort, S.; Kambhu, A. Developing persulfate-activator soft solid (PASS) as slow release oxidant to remediate phenol-contaminated groundwater. *Environ. Technol. Innov.* **2021**, *22*, 101396. [CrossRef]

24. Ma, J.; Ma, Y.; Rong, X.; Song, Q.; Wu, B.; Lan, X.; Feng, Y.; Qiu, X.; Zhang, P. Persulfate-based controlled release beads for in situ chemical oxidation of common organic pollutants. *J. Environ. Chem. Eng.* **2021**, *9*, 105627. [CrossRef]
25. Zha, P.; Yu, F.; Wang, R.; Ma, Y.; Wu, Y. Sodium alginate/graphene oxide hydrogel beads as permeable reactive barrier material for the remediation of ciprofloxacin-contaminated groundwater. *Chemosphere* **2018**, *200*, 612–620. [CrossRef] [PubMed]
26. Wang, B.; Zhang, Y.; Gao, C.; Du, X.; Qu, T. Developing novel persulfate pellets to remediate BTEXs-contaminated groundwater. *J. Water. Process Eng.* **2023**, *52*, 103505. [CrossRef]
27. Retno, A.; Putri, W.; Hasan, M.; Sari, E.; Taufik, A.; Lisna, E. Environmentally friendly slow-release urea fertilizer based on modified chitosan membrane. *Environ. Nanotechnol, Monit. Manag.* **2024**, *22*, 100996. [CrossRef]
28. Kim, H.W.; Jo, J.H.; Kim, Y.B.; Le, T.K.; Yeom, S.J. Biodegradation of polystyrene by bacteria from the soil in common environments. *J. Hazard. Mater.* **2021**, *416*, 126239. [CrossRef]
29. Zhang, W.; Wang, C.; Fang, M.; Li, B.; Jia, J.; Yu, B.; Wang, L. Highly effective flame-retardant coatings consisting of urea-formaldehyde resin/aluminium hydroxide/boric acid for polystyrene foam: Properties and mechanisms investigation. *Prog. Org. Coat.* **2024**, *196*, 108766. [CrossRef]
30. Hasanzadeh, R.; Azdast, T.; Mojaver, M.; Park, C.B. High-efficiency and low-pollutant waste polystyrene and waste polystyrene foam gasification: Comprehensive comparison analysis, multi-objective optimization and multi-criteria decision analysis. *Fuel* **2022**, *316*, 123362. [CrossRef]
31. Alsalem, S.M.; Lettieri, P.; Baeyens, J. Recycling and recovery routes of plastic solid waste (PSW) A review. *Waste Manag.* **2009**, *29*, 2625–2643. [CrossRef]
32. Kytinou, V.K.; Metaxa, Z.S.; Zapris, A.G.; Kosheleva, R.I.; Prokopiou, V.D.; Alexopoulos, N.D. Exploitation of extruded polystyrene (XPS) waste for lightweight, thermal insulation and rehabilitation building applications. *Dev. Built Environ.* **2024**, *20*, 100580. [CrossRef]
33. Maria, A.D.; Ramon, A. Advances in the recycling of plastic wastes for metallurgical coke production. *J. Mater. Cycles Waste Manag.* **2013**, *15*, 247–255. [CrossRef]
34. Holtkamp, M.; Renner, M.; Matthiesen, K.; Wald, M.; Luinstra, G.A.; Biessey, P. Robust downstream technologies in polystyrene waste pyrolysis: Design and prospective life-cycle assessment of pyrolysis oil reintegration pathways. *Resour. Conserv. Recycl.* **2024**, *205*, 107558. [CrossRef]
35. Shah, S.T.; Haq, F.U.; Hussain, T.; Bajwa, S.Z.; Bekchanov, D.; Din, M.I.; Mujahid, A.; Afzal, A. Expanded polystyrene (EPS) waste upcycling and efficient oil/water emulsion separation with advanced EPS-cotton membranes. *Desalin. Water Treat.* **2024**, *320*, 100647. [CrossRef]
36. Kol, R.; Carrieri, E.; Gusev, S.; Verswyvel, M.; Niessner, N.; Lemonidou, A.A.; Achilias, D.S.; De Meester, S. Removal of undissolved substances in the dissolution-based recycling of polystyrene waste by applying filtration and centrifugation. *Sep. Purif. Technol.* **2023**, *325*, 124682. [CrossRef]
37. Hamad, K.; Kaseem, M.; Deri, F. Recycling of waste from polymer materials: An overview of the recent works. *Polym. Degrad. Stab.* **2013**, *98*, 2801–2812. [CrossRef]
38. Chumbhale, V.R.; Kim, J.S.; Lee, S.B.; Choi, M.J. Catalytic degradation of expandable polystyrene waste (EPSW) over mordenite and modified mordenites. *J. Mol. Catal. A Chem.* **2004**, *222*, 133–141. [CrossRef]
39. María, T.G.; Ignacio, G.F.; Duque, G.; Antonio, L.M.; Juan, F.R. Study of the solubility and stability of polystyrene wastes in a dissolution recycling process. *Waste Manag.* **2009**, *29*, 1814–1818. [CrossRef]
40. Akanji, I.O.; Iwarere, S.A.; Sani, B.S.; Mukhtar, B.; Jibril, B.E.; Daramola, M.O. Polystyrene-reduced graphene oxide composite as sorbent for oil removal from an Oil-Water mixture. *Chem. Eng. Sci.* **2024**, *298*, 120383. [CrossRef]
41. Rostamipoor, H.; Ahmadi, H.; Haddadi-Asl, V.; Moussaei, M.; Roghani-Mamaqani, H. Synthesis of magnetic polystyrene nanocomposite by emulsion polymerization using a photo-responsive emulsifier for efficient crude oil absorption. *J. Photochem. Photobiol. A Chemisrty* **2025**, *459*, 116092. [CrossRef]
42. Chen, A.; Gong, M.; Chi, J.; Wang, Z.; Dai, L. Exploring the Potential Mechanisms of the Ethyl Acetate Fraction of *Hippophae rhamnoides* L. Seeds as a Natural Healing Agent for Wound Repair. *J. Ethnopharmacol.* **2024**, *14*, 118688. [CrossRef]
43. Wagner, C. Diffraction studies of the structure of amorphous and nanocrystalline metals and alloys: A review. *J. Non-Cryst. Solids* **1992**, *150*, 1–9. [CrossRef]
44. Zhang, N.; Sánchez-Montes, I.; Luo, H.; Qu, L.; Wang, J.; Chelme-Ayala, P.; Mohamed, G. Activation of persulfate by visible-light-driven Fe(ii)/Fe(iii) cycle of ferric citrate for decomplexation of cu(ii)-EDTA. *J. Water Process Eng.* **2024**, *63*, 105484. [CrossRef]
45. Wang, P.; Zhang, X.; Zhang, X.; Du, P.; Zhou, B.; Meng, F.; Wei, C.; Zhou, L.; Wen, G.; Wang, Y. Manganese oxide catalytic materials for degradation of organic pollutants in advanced oxidation processes: A review. *J. Water Process Eng.* **2024**, *66*, 106048. [CrossRef]

46. Xie, X.; Zhang, Y.; Huang, W.; Huang, S. Degradation kinetics and mechanism of aniline by heat-assisted persulfate oxidation. *J. Environ. Sci.* **2012**, *24*, 821–826. [CrossRef] [PubMed]
47. Wu, Y.; Guo, J.; Han, Y.; Zhu, J.; Zhou, L.; Lan, Y. Insights into the mechanism of persulfate activated by rice straw biochar for the degradation of aniline. *Chemosphere* **2018**, *200*, 373–379. [CrossRef] [PubMed]